Temporal-dependent effects of rainfall characteristics on inter-/intra-event branch-scale stemflow variability in two xerophytic shrubs

Chuan Yuan[1, 2, 4], Guangyao Gao[2,3], Bojie Fu[2,3], Daming He[1, 4], Xingwu Duan[1, 4], and Xiaohua Wei[5]

[1]Institute of International Rivers and Eco–security, Yunnan University, Kunming 650091, China

[2]State Key Laboratory of Urban and Regional Ecology, Research Center for Eco-Environmental Sciences, Chinese Academy of Sciences, Beijing 100085, China

[3]University of Chinese Academy of Sciences, Beijing 100049, China

[4]Yunnan Key Laboratory of International Rivers and Trans-boundary Eco–security, Kunming 650091, China

[5]Department of Earth, Environmental and Geographic Sciences, University of British Columbia (Okanagan campus), Kelowna, British Columbia, V1V 1V7, Canada

Correspondence: Guangyao Gao **(**gygao@rcees.ac.cn)

Abstract

Stemflow is important for recharging root-zone soil moisture in arid regions. Previous studies have generally focused on stemflow volume, efficiency and influential factors but have failed to depict stemflow processes and quantify their relations with rainfall characteristics within events, particularly for xerophytic shrubs. Here, we measured the stemflow volume, intensity, funnelling ratio, and time lags to rain at two dominant shrub species (*Caragana korshinskii* and *Salix psammophila*) and rainfall characteristics during 54 events at the semi-arid Liudaogou catchment of the Loess Plateau, China, during the 2014–2015 rainy seasons. Funnelling ratio was calculated as the ratio between stemflow and rainfall intensities at the inter-/intra-event scales. Our results indicated that the stemflow of *C. korshinskii* and *S. psammophila* were averagely started 66.2 and 54.8 min, maximized 109.4 and 120.5 min after rains began, and ended 20.0 and 13.5 min after rains ceased. The two shrubs had shorter stemflow duration (3.8 and 3.4 h) and significantly larger stemflow intensities (517.5 and 367.3 $mm\cdot h^{-1}$) than those of rains (4.7 h and 4.5 $mm\cdot h^{-1}$). As branch size increased, both species shared the decreasing funnelling ratios (97.7–163.7 and 44.2–212.0) and stemflow intensities (333.8–716.2 $mm\cdot h^{-1}$ and 197.2–738.7 $mm\cdot h^{-1}$). Tested by the multiple correspondence analysis and stepwise regression, rainfall amount and duration controlled stemflow volume and duration, respectively, at event scale by linear relations (p<0.01). Rainfall intensity and raindrop momentum controlled stemflow intensity and time lags to rains for both species within event by linear or power relationships (p<0.01). Rainfall intensity was the key factor affecting stemflow process of *C. korshinskii*, whereas raindrop momentum had the greatest influence on stemflow process of *S. psammophila*. Therefore, rainfall characteristics had temporal-dependent influences on corresponding stemflow variables, and the influence also depended on specific species.

1 Introduction

Stemflow directs the intercepted rains from canopy to the trunk base. The funnel-shaped canopy and underground preferential paths, i.e., roots, worm paths and soil macropores, converge rains to recharge the root-zone moisture (Johnson and Lehmann, 2006; Li et al., 2008). Stemflow is important to concentrate water (Levia and Germer, 2015), nutrients (Dawoe et al., 2018), pathogens (Garbelotto et al., 2003) and bacteria (Bittar et al., 2018) from the phyllosphere into the pedosphere (Teachey et al., 2018), even though stemflow accounts for only a minor part of rainfall amount (RA) (6.2%) in contrast to throughfall (69.8%) and interception loss (24.0%) in dryland ecosystems with annual mean rainfall ranging in 154–900 mm (Magliano et al., 2019). Stemflow greatly contributes to the survival of xerophytic plant species (Návar, 2011), the maintenance of patch structures in arid areas (Kéfi et al., 2007), and the normal functioning of rainfed dryland ecosystems (Wang et al., 2011).

To quantify the ecohydrological importance of stemflow, numerous studies have been conducted on stemflow production and efficiency from various aspects, including stemflow volume (mL), depth (mm), percentage (%), funnelling ratio (unitless), and productivity ($mL \cdot g^{-1}$, the branch stemflow volume of unit biomass) (Herwitz, 1986; Yuan et al., 2016; Zabret et al., 2018; Yang et al., 2019). By installing automatic recording devices, the stemflow process has been gradually determined at 1-h intervals (Spencer and van Meerveld, 2016), 5-min intervals (André et al., 2008; Levia et al., 2010) and 2-min intervals (Dunkerley, 2014b). This determination allowed to compute stemflow intensity ($mm \cdot h^{-1}$) (Germer et al., 2010), flux ($mL \cdot min^{-1}$) (Yang, 2010) and time lag after rain (Cayuela et al., 2018). Differing from an event-based calculation, the stemflow process provided insights into the fluctuation of stemflow production at a high temporal resolution. It permits a better interpretation of the "hot moment" and "hot spot" effects of many ecohydrological processes (Bundt et al., 2001; McClain et al., 2003). Quantifying the short-intensity burst and temporal characteristics shed light on the dynamic process and pulse nature of stemflow (Dunkerley, 2019).

Stemflow cannot be initiated until canopies were saturated by the rains (Martinez-Meza and Whitford, 1996). The minimal RA needed to start stemflow was usually calculated by regressing stemflow volume with RA at different plant species (Levia and Germer, 2015). It also varied with canopy states, i.e., 10.9 and 2.5–3.4 mm for the leafed oak and beech tress, and 6.0 mm and 1.5–1.9 mm for them in the leafless period (André et al., 2008; Staelens et al., 2008). Stemflow also frequently continued after rains ceased due to the rainwater retained on the canopy/branch surface (Iida et al., 2017). *Salix psammophila* and an open tropical forest started stemflow 5–10 min and 15 min later than the beginning of a rain event in the Mu Us desert of China (Yang, 2010) and the Amazon basin of Brazil (Germer et al., 2010), respectively. However, 1 h and 1.5 h were needed to start stemflow after the beginning of a rain event for pine and oak trees in north-eastern Spain, respectively (Cayuela et al., 2018). For *S. psammophila*, stemflow flux was maximized 20–210 min after the beginning of a rain event (Yang, 2010), and stemflow ceased 11 h after rains ceased in an open tropical forest (Germer et al., 2010). Time lags of stemflow generation, maximization and ending to rains depicted dynamic stemflow process, and were conducive to better understand the hydrological process occurred at the interface between the intercepted rains and soil moisture (Sprenger et al., 2019). It was important to discuss the temporal persistence in spatial patterns of soil moisture particularly at the intra-event scale (Gao et al., 2019). However, stemflow time lags have not been systematically studied for xerophytic shrubs.

The preferential paths at the underside of branches for delivering stemflow complicates stemflow processes within events (Dunkerley, 2014a). The influences of bark microrelief on stemflow are strongly affected by dynamic rain processes, such as rainfall intensity and raindrop striking within events (van Stan and Levia, 2010). While exceeding the holding capacity of branches, high rainfall intensity could overload and interrupt this preferential path (Carlyle-Mose and Price, 2006). Raindrops hit the canopy surface and create splashes on the surface. This process is conducive to wetting branches at the lower layers and accelerating the establishment of the preferential paths of stemflow transportation (Bassette and Bussière, 2008). Nevertheless, the interaction between the stemflow process and intra-event rainfall characteristics has not been substantially studied.

This study was designed at the event and process scales to investigate inter-/intra-event stemflow variability of two dominant xerophytic shrubs. Stemflow volume, intensity, funnelling ratio and temporal dynamics of *Caragana korshinskii* and *S. psammophila* were recorded during the 2014–2015 rainy seasons on the Loess Plateau of China. Temporal dynamics were expressed as stemflow duration and time lags of stemflow generation, maximization and cessation to rains. Raindrop momentum was introduced to represent the comprehensive effects of raindrop size, velocity, inclination angle and kinetic energy at the stemflow process. Funnelling ratio had been calculated at the event base and the 100-s intervals to assess the convergence effects of stemflow. This study specifically aimed to (1) depict the stemflow process in terms of stemflow intensity and temporal dynamics, (2) identify the dominant rainfall characteristics influencing inter-/intra-event stemflow variables, and (3) quantify the relationships between stemflow process variables and rainfall characteristics. Achieving these objectives would advance our knowledge of the process-based stemflow production to better understand the pulse nature of stemflow and its interactions with dynamic rain processes.

2 Materials and Methods

2.1 Site description

This study was conducted in the Liudaogou catchment (110°21′–110°23′E, 38°46′–38°51′N) in Shenmu city, Shaanxi Province, China, during the 2014–2015 rainy seasons. This catchment is 6.9 km^2 and 1094–1273 m above sea level (m.a.s.l.). A semiarid continental climate prevails in this area. The mean annual precipitation (MAP) is 414 mm (1971–2013). Most MAP (77%) occurs from July to September (Jia et al., 2013). The mean annual potential evaporation is 1337 mm (Yang et al., 2019). The mean annual temperature is 9.0 °C. The dominant shrubs include *C. korshinskii*, *S. psammophila*, and *Amorpha fruticosa*. The dominant grasses are *Artemisia capillaris*, *Artemisia sacrorum*, *Medicago sativa*, *Stipa bungeana*, etc.

C. korshinskii and *S. psammophila* are dominant shrub species at the arid and semi-arid regions of northwestern China (Hu et al., 2016; Liu et al., 2016). They were commonly planted for soil and water conservation, sand fixation and wind barrier, and had extensive distributions at this region (Li et al., 2016). The both species have inverted-cone crowns and no trunks, with multiple branches running obliquely from the base. As modular organisms and multi-stemmed shrub species, their branches live as independent individuals and compete with each other for water and light (Firn, 2004). Two plots were established in the southwestern catchment for these two xerophytic shrubs planted in the 1990s (Fig. 1). *C. korshinskii* and *S. psammophila* plots share similar stand conditions with elevations of 1179 and 1207 m.a.s.l., slopes of 13° and 18°, and sizes of 3294 and 4056 m^2, respectively. The *C. korshinskii* plot has a ground surface of loess and aspect of 224°, while the *S. psammophila* plot has a ground surface of sand and an aspect of 113°.

2.2 Meteorological measurements and calculations

A meteorological station was installed at the experimental plot of *S. psammophila* to record rainfall characteristics and wind speed (WS, $m \cdot s^{-1}$) (Model 03002, R. M. Young Company, USA), air temperature (T, °C) and relative humidity (H, %) (Model HMP 155, Vaisala, Finland). They were logged at 10-min intervals by a datalogger (Model CR1000, Campbell Scientific Inc., USA). Evaporation coefficient (E, unitless) was calculated to present the evaporation intensity (Equations 1–3) via aerodynamic approaches (Carlyle-Mose and Schooling, 2015). Tipping-bucket rain gauges (hereinafter referred to as "TBRG") automatically recorded the volume and timing of rainfall and stemflow (Herwitz, 1986; Germer et al., 2010; Spencer and Meerveld, 2016; Cayuela et al., 2018). To mitigate the systematic errors for missing the records of inflow during tipping intervals (Groisman and Legates, 1994), we chose the Onset® (Onset Computer Corp., USA) RG3-M TBRG with the relatively smaller underestimation for its smaller bucket volume (3.73±0.01 mL) (Iida et al., 2012). Besides, three 20-cm-diameter standard rain gauges were placed around TBRG with a 0.5-m distance at the 120° separation (Fig. 1). The regression (R^2=0.98, *p*<0.01) between manual measurements and automatic recording further mitigated the understanding of inflow water by applying TBRG (Equation 4).

$$e_s = 0.611 \times \exp\left(17.27 \times T \big/ \left(237.7 + T\right)\right) \tag{1}$$

$$VPD = e_s \times \left(1 - H\right) \tag{2}$$

$$E = WS \times VPD \tag{3}$$

where e_s is the saturation vapor pressure (kPa); T is air temperature (°C); H is air relative humidity (%); VPD is the vapor pressure deficit (kPa); and E is the evaporation coefficient (unitless).

$$IW_A = IW_R \times 1.32 + 0.16 \tag{4}$$

where IW_R is the recording of inflow water (including rainfall and stemflow) via TBRG (mm), and IW_A is the adjusted inflow water (mm).

Discrete rainfall events were defined by a measurable RA of 0.2 mm (the resolution limit of the TBRG) and the smallest 4-h gap without rains. That was the same period of time to dry canopies from antecedent rains as reported by Giacomin and Trucchi (1992), Zhang et al. (2015), Zhang et al., (2017) and Yang et al. (2019). Rainfall interval (RI, h) was calculated to indirectly represent the bark wetness. Other rainfall characteristics were also computed, including the RA (mm), rainfall duration (RD, h), the average and 10-min maximum rainfall intensity of incident rains (I and I_{10}, $mm \cdot h^{-1}$), and the 10-min average rainfall intensity after rain begins (I_{b10}, $mm \cdot h^{-1}$) and before rain ends (I_{e10}, $mm \cdot h^{-1}$). By assuming a perfect sphere of a raindrop (Uijlenhoet and Torres, 2006), raindrop momentum in the vertical direction (F, $mg \cdot m \cdot s^{-1}$) (Equation 8–9) was computed to comprehensively represent the effects of raindrop size (D, mm) (Equation 5), terminal velocity (v, $m \cdot s^{-1}$)

(Equation 6), average inclination angle (θ, °) (Equation 7) affecting stemflow process (Brandt, 1990; Kimble, 1996; van Stan et al., 2011; Carlyle-Moses and Schooling, 2015). The 10-min maximum raindrop momentum (F_{10}, mg·m·s^{-1}) and the average raindrop momentum at the first and last 10 min (F_{b10} and F_{e10}, respectively, mg·m·s^{-1}) could be calculated with I_{10}, I_{b10} and I_{e10} as indicated at Equation 5–9, respectively. For the 0.8-km distance between the two plots, the meteorological data were used at the *C. korshinskii* plot.

$$D = 2.23 \times (0.03937 \times I)^{0.102} \quad (5)$$

$$v = 3.378 \times \ln(D) + 4.213 \quad (6)$$

$$\tan\theta = {WS}/{v} \quad (7)$$

$$F_0 = m \times v = ({1}/{6} \times \rho \times \pi \times D^3) \times v \quad (8)$$

$$F = F_0 \times \cos\theta \quad (9)$$

where D is raindrop diameter (mm); I is the average rainfall intensity of incident rains (mm·h^{-1}); v is raindrop velocity (m·s^{-1}); θ is average inclination angle of raindrops (°); WS is the average wind speed of incident rains (m·s^{-1}); F_0 is the average raindrop momentum (mg·m·s^{-1}); m is the average raindrop mass (g); ρ is the density of freshwater at standard atmospheric pressure and 20°C (0.998 g·cm^{-3}).

2.3 Experimental branch selection and measurements

This study focused on the branch-scale stemflow production of the 20-year-old *C. korshinskii* and *S. psammophila*. Based on plot investigation, the canopy traits of standard shrubs were determined. Four shrubs were selected accordingly at each species with similar crown areas and heights (5.1±0.3 m^2 and 2.1±0.2 m for *C. korshinskii* and 21.4±5.2 m^2 and 3.5±0.2 m for *S. psammophila*, respectively). The approximately 10-m gap between them guaranteed shrubs exposing to the similar meteorological conditions (Yuan et al., 2016). We measured branch morphologies of all 180 and 261 branches at experimental shrubs of *C. korshinskii* and *S. psammophila*, respectively, including BD (Basal diameter, mm) with a Vernier calliper (Model 7D-01150, Forgestar Inc., Germany), branch length (BL, cm) with a measuring tape, and branch angle (BA, °) with pocket geologic compass (Model DQL-8, Harbin Optical Instrument Factory, China), respectively. Thus, BD categories were determined at 5–10 mm, 10–15 mm, 15–18 mm, 18–25 mm and >25 mm to guarantee the appropriate branch amounts within categories for meeting the statistical significance. Two representative branches with median BDs were selected in each category for stemflow recording. The experimental branches had no intercrossing with neighbouring ones and no turning point in height from branch tip to base. The outlayer-of-canopy positions avoided over-shading by the upper layer branches and permitted convenient measurements. Since the qualified branch with the >25-mm size was not enough for *C. korshinskii* and the TBRG malfunctioned at the 15–18-mm branches of *S. psammophila*, stemflow data were not available in these BD categories. In total, 7 branches were selected for stemflow measurements at each species (Table 1). As the important interface to intercept rains at the growing season, the well-verified allometric growth equations were performed to estimate the branch leaf area (LA, cm^2) of *C korshinskii* ($LA=39.37\times BD^{1.63}$ R^2=0.98) (Yuan et al., 2017) and *S. psammophila* ($LA=18.86\times BD^{1.74}$ R^2=0.90) (Yuan et al., 2016), respectively.

2.4 Stemflow measurements and calculations

A total of 14 TBRGs had been applied to automatically record the branch stemflow production of *C. korshinskii* and *S. psammophila*. The data of stemflow volume and timing were automatically recorded at dynamic intervals between neighboring tips. We installed aluminium foil collars to trap stemflow at branches nearly 40 cm off the ground, higher than TBRG orifice with height of 25.7 cm (Fig. 1). They were fitted around the entire branch circumference and sealed by neutral silicone caulking. The limited orifice diameter of foil collars minimized the accessing of throughfall and rains into them (Yuan et al., 2017). The 0.5-cm-diameter polyvinyl chloride hoses hung vertically and channelled stemflow from the collars to TBRGs with a minimum travel time. TBRGs were covered with the polyethylene films to prevent the accessing of throughfall and splash (Fig. 1). These apparatuses were periodically checked against leakages or blockages by insects and fallen leaves. Stemflow variables were computed as follow.

(1) Stemflow volume (SFV, mL): the average stemflow volume of individual branches. Adjusted with Equation 4 firstly, SFV was computed with the TBRG recordings (SF_{RG}, mm) by multiplying its orifice area (186.3 cm^2) (Equation 10).

$$SFV = SF_{RG} \times 18.63 \qquad (10)$$

(2) Stemflow intensity: the branch stemflow volume per branch basal area per unit time. SFI ($mm \cdot h^{-1}$) is the average stemflow intensity of incident rains, which is computed by the event-based SFV (mL), branch basal area (BBA, mm^2) and RD (h) (Equation 11) (Herwitz, 1986; Spencer and Meerveld, 2016). SFI_{10} ($mm \cdot h^{-1}$) is the 10-min maximum stemflow intensity, which is calculated with the 10-min maximum stemflow volume (SFV_{10}, mL) and BBA (mm^2) (Equation 12). SFI_i ($mm \cdot h^{-1}$) is the instantaneous stemflow intensity, which is calculated by the tip volume of TBRG (3.73 mL), BBA (mm^2) and time intervals between neighbouring

tips (t_i, h) (Equation 13). The comparison between SFI_i and the corresponding rainfall intensity depicted the synchronicity of stemflow with rains within event.

$$SFI = 1000 \times SFV / (BBA \times RD) \tag{11}$$

$$SFI_{10} = 6000 \times SFV_{10} / BBA \tag{12}$$

$$SFI_i = 3730 / \left(BBA \times t_i\right) \tag{13}$$

(3) Stemflow temporal dynamics: stemflow duration and time lags to rains.

SFD (h): stemflow duration. It is computed by different timings between the first- and last-tips of stemflow via TBRG.

TLG (min): time lag of stemflow generation after rain begins. It is computed by different first-tip timings between rainfall and stemflow via TBRG.

TLM (min): time lag of stemflow maximization after rain begins. It is computed by different timings between the largest-SFI_i and first-rainfall tips via TBRG.

TLE (min): time lag of stemflow ending after rain ceases. It is computed by different last-tip timings between rainfall and stemflow via TBRG.

(4) Funnelling ratio: the efficiency for capturing and delivering raindrops from the canopies to trunk/branch base (Siegert and Levia, 2014; Cayuela et al., 2018). By introducing RD at both numerator and denominator of the original equation (Herwitz, 1986), FR (unitless) was transformed as the ratio between stemflow and rainfall intensities at the event base (Equation 14). FR_{100} described the within-event funnelling ratio at the 100-s interval after rain began (Equation 15).

$$FR = 1000 \times \frac{SFV}{BBA \times RA} = 1000 \times \frac{\frac{SFV}{BBA} / RD}{RA / RD} = \frac{SFI}{I} \tag{14}$$

$$FR_{100_i} = SFI_{100_i} / I_{100_i} \quad (15)$$

where FR_{100i}, SFI_{100i} and I_{100i} are funnelling ratio, stemflow intensity and rainfall intensity at the internal *i* with 100-s pace after rain begins, respectively.

2.5 Data analysis

Stemflow variables were averaged at different BD categories to analyse the most influential rainfall characteristics affecting them. Pearson correlation analyses were firstly performed to test the relationships between rainfall characteristics (RA, RD, RI, I, I_{10}, I_{b10}, I_{e10}, F, F_{10}, F_{b10}, F_{e10} and E) and stemflow variables (SFV, SFI, SFI_{10}, FR, TLG, TLM, TLE and SFD). The significantly related factors were grouped in terms of median value, and compiled into indicator matrices. They were standardized for a cross-tabulation check as required by the multiple correspondence analysis (MCA) (Levia et al., 2010; van Stan et al., 2011, 2016). All qualified data were restructured into orthogonal dimensions (Hair et al., 1995), where distances between row and column points were maximized (Hill and Lewicki, 2007). As shown at correspondence maps, the clustering rainfall characteristics tightly related to the centred stemflow variable. Finally, stepwise regressions were operated to identify the most influential rainfall characteristics (Carlyle-Moses and Schooling, 2015). The quantitative relations were established in terms of the qualified level of significance (p <0.05) and the highest coefficient of determination (R^2). One-way analysis of variance (ANOVA) with LSD post hoc test was used to determine whether rainfall characteristics， and stemflow variables significantly differed among event categories, and whether funnelling ratio and stemflow intensity significantly differed among BD categories for *C. korshinskii* and *S. psammophila*. The level of significance was set at 95% confidence interval (p=0.05). SPSS 21.0 (IBM Corporation, USA), Origin 8.5 (OriginLab Corporation, USA) and Excel 2019 (Microsoft Corporation, USA) were used for data analysis.

3 Results

3.1 Rainfall characteristics

A total of 54 rainfall events had been recorded for stemflow measurements at the 2014–2015 rainy seasons (Fig. 2). Thereinto, 20, 8, 10, 8, 4 and 4 events were at the RA categories of ≤2 mm, 2–5 mm, 5–10 mm, 10–15 mm, 15–20 mm and >20 mm, respectively. The total RAs at these categories were 22.1 mm, 26.1 mm, 68.8 mm, 93.3 mm, 74.8 mm and 110.0 mm, respectively. During these events, the average I, I_{10}, I_{b10} and I_{e10} were 4.5±1.0 mm·h^{-1}, 10.9±2.1 mm·h^{-1}, 5.5±1.4 mm·h^{-1} and 2.8±0.7 mm·h^{-1}, respectively. The average F, F_{10}, F_{b10} and F_{e10} were 16.1±1.2 mg·m·s^{-1}, 24.9±1.4 mg·m·s^{-1}, 18.4±1.4 mg·m·s^{-1} and 16.0±1.0 mg·m·s^{-1}, respectively. RD, RI and E averaged 4.7±0.8 h, 50.6±6.1 h, and 0.9±0.2, respectively (Table 2).

Rainfall events were further categorized in terms of rainfall-intensity peak amount, including Events A (the single-peak events), B (the double-peak events) and C (the multiple-peak events). There were 17, 11 and 15 events at Event A, B and C, respectively. Because the remaining 11 events had the average RA of 0.6 mm, no more than three recordings had been observed within event which was limited by 0.2-mm resolution of TBRGs. Therefore, they could not be categorized and grouped as Event others (Table 2). Compared with Events A and B, Event C possessed significantly different rainfall characteristics, e.g., the significantly larger RA (11.7 vs. 4.1 and 5.2 mm) and RD (10.3 vs. 2.5 and 3.6 h) but the significantly smaller I_{10} (9.5 vs. 15.5 and 12.7 mm·h^{-1}), I_{b10} (2.8 vs.

7.7 and 9.9 mm·h^{-1}), F_{b10} (15.4 vs. 19.7 and 21.7 mg·m·s^{-1}) and F_{e10} (13.4 vs. 17.3 and 16.6 mg·m·s^{-1}), the non-significantly smaller I_{e10} (2.1 vs. 4.3 and 3.6 mm·h^{-1}), F_{10} (24.2 vs. 27.8 and 26.6 mg·m·s^{-1}) and E (0.4 vs. 0.9 and 1.0), respectively (Table 2).

In general, rainfall events were skewedly distributed in terms of RA. The occurrences of events with a RA≤2 mm dominated the experimental period (40.7%), but the events with RA>20 mm were the greatest contributor to the total RA (28.0%). However, a relatively equal distribution was noted during events with single (17 events), double (11 events) and multiple (15 events) rainfall-intensity peaks. Comparatively, the multiple-peak events had significantly larger rainfall amounts, durations, intensities and raindrop momentums.

3.2 Inter-/intra-event stemflow variability

Stemflow variables of *C. korshinskii* and *S. psammophila* showed great inter-event variations during the experimental period (Fig. 3). *C. korshinskii* had larger SFV, SFI, SFI_{10}, FR, SFD, TLG and TLE (226.6±46.4 mL, 517.5±82.1 mm·h^{-1}, 2057.6±399.7 mm·h^{-1}, 130.7±8.2, 3.8±0.8 h, 66.2±10.6 min and 20.0±5.3 min, respectively) but smaller TLM (109.4±20.5 min) than those of *S. psammophila* (172.1±34.5 mL, 367.3±91.1 mm·h^{-1}, 1132.2±214.3 mm·h^{-1}, 101.6±10.4, 3.4±0.9 h, 54.8±11.7 min, 13.5±17.2 min, and 120.5±22.1 min, respectively) (Table 3). During the 54 events, no negative values were observed for TLG and TLM but TLE. It indicated that stemflow generally initiated and maximized after rains started for both species. However, stemflow might be ended before (negative TLE) and after (positive TLE) rains ceased.

Stemflow well synchronized to rains with similar intensity peak shapes, amounts and positions for both species. These results were vividly demonstrated at representative rains with different intensity peak amounts and RAs, including events on July 17, 2015 (Event A, 20.7 mm), July 29, 2015 (Event B, 7.3 mm), and September 10, 2015 (Event C, 13.3 mm) (Fig. 4). *C. korshinskii* had larger FR_{100} (91.7, 76.1 and 94.0, respectively) than those of *S. psammophila* (32.8, 26.3 and 43.7, respectively) during representative events. It indicated a comparatively greater ability of converging rains for *C. korshinskii* within event.

Stemflow variables varied between rainfall event categories. For Event C in comparison to Events A and B, *S. psammophila* had significantly larger SFV (435.2 vs. 102.6 and 145.7 mL), SFD (8.3 vs. 1.2 and 3.4 h), TLM (235.8 vs. 64.3 and 93.4 min), FR (129.1 vs. 77.1 and 91.4), non-significantly larger TLE (20.8 vs. 17.1 and 8.6 min) but significantly smaller SFI (246.6 vs. 648.1 and 421.5 mm·h^{-1}) and SFI_{10} (888.4 vs. 1672.7 and 1582.8 mm·h^{-1}), respectively (Table 3). SFI decreased at events with increasing intensity peak amounts as shown at Events A–C. The drop of SFI was offset by the decreasing I to some extent (Table 2), which might partly explain the increasing trend of FR from Event A to C. *C. korshinskii* shared similar changing trends of stemflow variables between event categories with those of *S. psammophila*, except for the non-significantly smaller TLE (18.5 min) at Event C in contrast to TLE at Event A and B (22.3 and18.7 min).

Funnelling ratio and stemflow intensity negatively related with branch size. *C. korshinskii* and *S. psammophila* had significantly greater FR, SFI, and SFI_{10} at the 5–10 mm branches than those at the larger branches (Table 4). For *C. korshinskii*, FR decreased from 163.7±12.2 at the 5–10-mm branches to 97.7±9.2 at the 18–25-mm branches, respectively. It was consistent with decreasing SFI (333.8–716.2 mm·h^{-1}) at the corresponding BD categories (Table 4). As branch size increased, *S. psammophila* shared similar decreasing trends of FR (44.2–212.0) and SFI (197.2–738.7 mm·h^{-1}), respectively.

3.3 Relationships between stemflow variables and rainfall characteristics

C. korshinskii and *S. psammophila* had similar correspondence patterns between rainfall characteristics and stemflow variables. As shown in Fig. 5, the one-to-one correspondences were observed for SFV and TLE. The larger (or smaller) SFV and TLE corresponded to the larger (or smaller) RA and RI, respectively. This result demonstrated the dominant influences of RA and RI on SFV and TLE, respectively. The one-to-two correspondences was noted for SFD with RD and E. The larger (or smaller) SFD corresponded to the larger (or smaller) RD and smaller (or larger) E. RA had been identified as the dominant rainfall characteristic affecting FR based on the analysis for 53 branches of *C. korshinskii* and 98 branches of *S. psammophila* at the same plots during the same experimental period (Yuan et al., 2017). It seemed that event-based stemflow production (the volume, duration and efficiency) were strongly influenced by rainfall characteristics at inter-event scale (the rainfall amount and duration).

The one-to-more correspondences were observed for TLM, TLG, SFI and SFI_{10} (Fig. 5). The larger (or smaller) TLM corresponded to the smaller (or larger) rainfall characteristics of I, I_{10}, I_{b10}, I_{e10}, F, F_{10}, F_{b10} and F_{e10}. The same correspondences were applied to the larger (or smaller) TLG, and the smaller (or larger) SFI and SFI_{10}. It seemed that the within-event stemflow processes (SFI, SFI_{10}, TLG and TLM) were strongly affected by rainfall characteristics at intra-event scale (the rainfall intensity and raindrop momentum). Therefore, these results indicated that rainfall characteristics influenced stemflow variables at the corresponding temporal scales. This influence occurred at the inter-event scale between SFV and RA, FR and RA, SFD and RD, and at the intra-event scale for stemflow time lags (TLG and TLM) and intensities (SFI and SFI_{10}) with rainfall intensity (I, I_{10}, I_{b10} and I_{e10}) and raindrop momentum (F, F_{10}, F_{b10} and F_{e10}). The only exception was noted between TLE and RI for the mismatched temporal sales.

Stepwise regression analysis identified the most influential rainfall characteristics affecting stemflow intensities and temporal dynamics. RD was the dominant rainfall characteristics affecting SFD. I_{10} significantly affected the TLM of the both species. For *C. korshinskii*, I, I_{10} and F were the most influential factors on SFI, SFI_{10} and TLG, respectively. However, for *S. psammophila*, F, F_{10} and F_{b10} significantly affected SFI, SFI_{10} and TLG, respectively. The results of multiple regression analysises indicated that there were linear relationships between SFI and I (R^2=0.74, p<0.01) and SFI_{10} and I_{10} (R^2=0.85, p<0.01) for *C. korshinskii* and between SFD and RD for *C. korshinskii* (R^2=0.95, p<0.01) and *S. psammophila* (R^2=0.92, p<0.01) (Fig. 6). Moreover, power functional relations were found between SFI and F (R^2=0.82, p<0.01), SFI_{10} and F_{10} (R^2=0.90, p<0.01) (Fig. 6), TLG and F_{b10} (R^2=0.55, p<0.01) and TLM and I_{10} (R^2=0.40, p<0.01) (Fig. 7) for *S. psammophila*, and TLG and F (R^2=0.56, p <0.01) and TLM and I_{10} (R^2=0.38, p<0.01) (Fig. 7) for *C. korshinskii*. However, there was no significant quantitative relationship between TLE and RI for *C. korshinskii* (R^2=0.005, p=0.28) or *S. psammophila* (R^2=0.002, p=0.78) (Fig. 7).

4 Discussion

4.1 Stemflow intensity and funnelling ratio

Stemflow intensity is generally greater than rainfall intensity at different plant life forms. The xerophytic shrubs of *C. korshinskii* and *S. psammophila* had larger average stemflow intensities than the average rainfall intensity (517.5 and 367.3 mm·h^{-1} vs. 4.5 mm·h^{-1}). Broadleaf and coniferous species (*Quercus pubescens* Willd. and *Pinus sylvestris* L., respectively) also have larger maximum stemflow intensities than the maximum rainfall intensity in north-eastern Spain (Cayuela et al., 2018). The gap between stemflow and rainfall intensities generally increased as the recording time intervals decreased. While recording at the 1-h intervals, approximately 20-, 17-, 13- and 2.5-fold greater peak stemflow intensities had been observed for trees of Cedar, Birch, Douglas Fir and Hemlock, respectively, at the coastal British Columbia forest (Spencer and Meerveld, 2016). For *C. korshinskii* and *S. psammophila*, in comparison to I_{10} (10.9 mm·h^{-1}) at 10-min intervals, the SFI_{10} (2057.6 and 1132.2 mm·h^{-1}, respectively) was over 103.9-fold greater. The recordings at 6-min interval indicated a 157-fold larger of stemflow intensity (18840 mm·h^{-1}) than rainfall intensity (120 mm·h^{-1}) in the cyclone-prone tropical rainforest with extremely high MAP of 6570 mm (Herwitz, 1986). While calculating the dynamic time interval between neighbouring tips of TBRG, SFI_i (10816.2 mm·h^{-1}) was 150.2-fold greater than the corresponding rainfall intensity (72 mm·h^{-1}). Therefore, stemflow recorded at a higher temporal resolution might provide more information into the dynamic nature of stemflow and real-time responses to rainfall characteristics within events.

Greater stemflow intensity than rainfall intensity is hydrologically significant at terrestrial ecosystems. This scenario indicates the convergence of the canopy-intercepted rains into the limited area around trunk or branch bases within a certain time period, i.e., 8.0% and 3.5% of rains being directed to the trunk base only accounting for 0.3% and 0.4% of plot area in the open rainforest (Germer et al., 2010) and undisturbed lowland tropical rainforest (Manfroi et al., 2004), respectively. Besides, FR, which compared SFV with RA that would have been collected at the same area as the basal area at an event scale (Herwitz, 1986), is commonly applied to assess the convergence effect via stemflow volume, rainfall amount and basal area (Carlyle-Moses et al., 2010; Siegert and Levia, 2014; Fan et al., 2015; Yang et al., 2019). If FR is greater than 1, more water is collected at the trunk or branch base than at the clearings. Both methods successfully quantified the convergence effects of stemflow. However, the former provided a possibility to assess it at high temporal resolutions within event.

This study established the quantitative connection between FR and stemflow intensity. As per Equation 14 and the average stemflow and rainfall intensities listed at Table 2 and 3, FR could be estimated to be 115.0 and 81.6 for *C. korshinskii* and *S. psammophila*, respectively. Those results approximately agreed with FR of 173.3 and 69.3 (Yuan et al., 2017) and 124.9 and 78.2 (Yang et al., 2019) for the two species by applying the traditional calculation based on SFV and RA (Herwitz, 1986). As branch size increased, FR of *C. korshinskii* decreased from 163.7 at the 5–10-mm branches to 97.7 at the 18–25-branches. The decreasing trend of FR of *S. psammophila* were also noted in the range of 44.2–212.0 with increasing BD. The negative relation between BD and FR agreed with the reports for trees and babassu palms in an open tropical rainforest in Brazil (Germer et al., 2010), the mixed-species coastal forest at British Columbia of Canada (Spencer and Meerveld, 2016), for trees (*Pinus tabuliformis* and *Armeniaca vulgaris*) and shrubs (*C. korshinskii* and *S. psammophila*) on the Loess Plateau of China (Yang et al., 2019). It might be partly explained by the decreasing stemflow intensities with increasing branch size as per

Equation 14. Our results found that SFI decreased from 716.2 to 333.8 for *C. korshinskii*, and 738.7 to 197.2 for *S. psammophila* as branch size increased (Table 4). It well justified the importance of branch size on stemflow intensity. Associated with the infiltration rate, the stemflow-induced hydrological process might be strongly affected, i.e., soil moisture recharge, Hortonian overland flow (Herwitz, 1986), saturation overland flow (Germer et al., 2010), soil erosion (Liang et al., 2011), nutrient leaching (Corti et al., 2019), etc. Therefore, more attention should be paid to tree/branch size and size-related stand age at future studies while modeling the stemflow-induced terrestrial hydrological fluxes.

The importance had been addressed to study the funnelling ratio at the stand scale (Carlyle-Moses et al., 2018); however, it had not been adequately studied at the intra-event scale. This study calculated the average funnelling ratio at the event base and the 100-s intervals after rain began. Thus, the convergence effect of stemflow could be better understood at the inter-/intra-event scales. Our results found that FR_{100} were over 1.8-fold greater than FR of *C. korshinskii* (282.7 vs. 130.7) and *S. psammophila* (203.4 vs. 101.6), respectively. It indicated that funnelling ratio fluctuated dramatically within event. Therefore, computing FR at event and ignoring it at high temporal resolutions within event might underestimate the eco-hydrological significance of stemflow.

In general, stemflow intensity highly related to funnelling ratio. For addressing its eco-hydrological importance, stemflow intensity should be precisely defined. It had been expressed as the stemflow volume per basal area of branches/trunks per unit time with the unit of $mm \cdot h^{-1}$ (Herwitz, 1986; Spencer and Meerveld, 2016) and $mm \cdot 5\ min^{-1}$ (Cayuela et al., 2018). However, stemflow intensity had also been described as stemflow volume per unit time with the unit of L·week^{-1} (Schimmack et al., 1993) and L·h^{-1} (Liang et al., 2011; Germer et al., 2013). We highly recommended the former definition. Because of its highly spatial-related attribution (Herwitz, 1986; Liang et al., 2011; 2014), the eco-hydrological significance of stemflow would be underestimated by ignoring the basal area, over which stemflow was received. Moreover, as per this definition, stemflow intensity quantitively connected with funnelling ratio via Equation 14. Thus, funnelling ratio could be used to assess the convergence effect of stemflow at both inter- and intra-event scales.

4.2 Stemflow temporal dynamics

Stemflow well synchronized to the rains. It agreed with the report of Levia et al. (2010), who demonstrated a marked synchronicity between SFV and RA in 5-min intervals for *Fagus. grandifolia*. The duration and time lags to rains were critical to describe stemflow temporal dynamics. Our results indicated that in comparison to *S. psammophila*, *C. korshinskii* takes a longer time to initiate (66.2 vs. 54.8 min), end (20.0 vs. 13.5 min) and produce stemflow (3.8 vs. 3.4 h) but a shorter time to maximize stemflow (109.4 vs. 120.5 min, respectively). Moreover, the TLMs of both species were in the range of the TLMs for *S. psammophila* (20–210 min) in the Mu Us desert of China (Yang, 2010).

Varying TLGs were documented for different species. Approximately 15 min, 1 h and 1.5 h were needed to initiate the stemflow of palms (Germer, 2010), pine trees and oak trees (Cayuela et al., 2018), respectively. In addition, an almost instantaneous start of stemflow had also been observed as rain began for *Quercus rubra* (Durocher, 1990), *Fagus grandifolia* and *Liriodendron tulipifera* (Levia et al., 2010). Compared to the positive TLE dominating xerophytic shrubs, the TLE greatly varied with tree species. TLE was as much as 48 h for Douglas fir, oak and redwood in California, USA (Reid and Levia, 2009), and almost 11 h for palm trees in Brazil (Germer, 2010). However, for sweet chestnut and oak, almost no stemflow continued when rains ceased in Bristol, England (Durocher, 1990). These scenarios might occur due to the sponge effect of the canopy surface (Germer, 2010), which buffered stemflow generation, maximization and cessation before saturation. These conclusions were consistent with the smaller stemflow intensities of *C. korshinskii* and *S. psammophila* than the rainfall intensity when rain began, as part of the rains was used to wet canopies (Fig. 4). The hydrophobic bark traits benefited stemflow initiation with the limited time lags to rains. In contrast, the hydrophilic bark traits were conducive for continuing stemflow after rain ceased, which kept the preferential flow paths wetter for longer time periods (Levia and Germer, 2015). As a result, it took time to transfer intercepted rains from the leaf, branch and trunk to the base. This process strongly affects the stemflow volume, intensity and loss as evaporation.

The dynamics of intra-event rainfall intensity complicated the stemflow time lags to rains. A 1-h lag to begin and stop stemflow with the beginning and ending of rains had been observed for ashe juniper trees during high-intensity events, but no stemflow was generated at low-intensity storms (Owens et al., 2006). Rainfall intensity was an important dynamic rainfall characteristic affecting stemflow volume. Owens et al. (2006) found the most significant difference between various rainfall intensities located in the stemflow patterns other than throughfall and interception loss. During events with a front-positioned, single rainfall-intensity peak, *S. psammophila* maximized stemflow in a shorter time than *C. korshinskii* did in the Mu Us desert (30 and 50 min) (Yang, 2010). These results highlighted the amounts and occurrence time of rainfall-intensity peak affecting the stemflow process, which was consistent with the finding of Dunkerley (2014b).

Raindrops presented rainfall characteristics at finer temporal-spatial scales. They were usually ignored because rains were generally regarded as a continuum rather than a discrete process consisting of individual raindrops of various sizes, velocities, inclination angles and kinetic energies. Raindrops hit the canopy surface and created splashes at different canopy layers (Bassette and Bussière, 2008; Li et al., 2016). This process accelerated canopy wetting and increased water supply for stemflow production. Therefore, raindrop momentum was introduced in this study to represent the comprehensive effects of raindrop attributes. Our results indicated that raindrop momentum was sensitive to predicting the variations in stemflow intensity and temporal dynamics with significant linear or power functional relations (Figs. 6 and 7). Compared with the importance of rainfall intensity for *C. korshinskii*, raindrop momentum more significantly affected the stemflow process of *S. psammophila*. This result might be related to the larger canopy size and height of *S. psammophila* (21.4±5.2 m^2 and 3.5±0.2 m) than that of *C. korshinskii* (5.1±0.3 m^2 and 2.1±0.2 m, respectively). More layers were available within canopies of *S. psammophila* to intercept the splashes created by raindrop striking (Bassette and Bussière, 2008; Li et al., 2016), thus shortening the paths and having more water supply for stemflow production.

4.3 Temporal-dependent influences of rainfall characteristics on stemflow variability

This study discussed stemflow variables and rainfall characteristics at inter-/intra-event scales. We found that rainfall characteristics affected stemflow variables at the corresponding temporal scales. RA and RD controlled SFV, FR and SFD, respectively, at the inter-event scale. However, stemflow intensity (e.g., SFI and SFI_{10}) and temporal dynamics (e.g., TLG and TLM) were strongly influenced by rainfall intensity (e.g., I, I_{10} and I_{b10}) and raindrop momentum (e.g., F, F_{10} and F_{b10}) at the intra-event scales. These results were verified by the well-fitting linear or power functional equations among them (Figs. 6 and 7). Furthermore, the influences of rainfall intensity and raindrop momentum on stemflow process were species-specific. In contrast to the significance of rainfall intensity on the stemflow process of *C. korshinskii*, raindrop momentum imposed a greater influence on the stemflow process of *S. psammophila*.

In general, rainfall characteristics had temporal-dependent influences on the corresponding stemflow variables. The only exception was found between TLE and RI. RI tightly corresponded to TLE for both species tested by the MCA, but there was no significant quantitative relationship between them (R^2=0.005, p=0.28 for *C. korshinskii*, and R^2=0.002, p=0.78 for *S. psammophila*). This result might be related to the mismatched temporal scales between TLE and RI. TLE represented stemflow temporal dynamics at the intra-event scale, while RI was the interval times between neighbouring rains at the inter-event scale. The mismatched temporal scales might also partly explain the long-standing debates on the controversial positive, negative and even no significant influences of rainfall intensity (depicting raining process at 5 min, 10 min, 60 min, etc.) on event-based stemflow volume (Owens et al., 2006; André et al., 2008; Zhang et al., 2015).

5 Conclusions

Stemflow intensity and temporal dynamics are important in depicting the stemflow process and its interactions with rainfall characteristics within events. We categorized stemflow variables into the volume, intensity, funnelling ratio and temporal dynamics, thus to representing the stemflow yield, efficiency and process. Funnelling ratio had been calculated as the ratio between stemflow and rainfall intensities, which enabled to assess the convergence of stemflow at the inter-/intra-event scales. Over 1.8-fold greater FR_{100} were noted than FR at representative events for *C. korshinskii* and *S. psammophila*, respectively. FR decreased with increasing branch size of both species. It could be partly explained by the decreasing trends of SFI as branch size increased. The rainfall characteristics had temporal-dependent influences on stemflow variables. RA and RD controlled SFV, FR and SFD at the inter-event scale. Rainfall intensity and raindrop momentum significantly affected stemflow intensity and time lags to rains at the intra-event scale except for TLE. The eco-hydrological significance of stemflow might be underestimated by ignoring stemflow production at high temporal resolutions within event. These findings advance our understanding of the stemflow process and its influential mechanism and help model the critical process-based hydrological fluxes of terrestrial ecosystems.

Data availability. The data collected in this study are available upon request to the authors.

Author contributions. GYG and CY set up the research goals and designed field experiments. CY measured and analyzed the data. GYG and BJF provided the financial support for the experiments, and supervised the execution. CY created the figures and wrote the original draft. GYG, BJF, DMH, XWD and XHW reviewed and edited the draft

in serval rounds of revision.

Competing interests. The authors declare that they have no conflict of interest.

Acknowledgements. This research was sponsored by the National Natural Science Foundation of China (nos. 41390462, 41822103 and 41901038), the National Key Research and Development Program of China (no. 2016YFC0501602), the Chinese Academy of Sciences (no. QYZDY-SSW-DQC025), the Youth Innovation Promotion Association CAS (no. 2016040), and the China Postdoctoral Science Foundation (no. 2018M633427). We appreciate Prof. D. F. Levia in University of Delaware for reviewing and improving this manuscript. Thanks to Liwei Zhang for the catchment GIS mapping. Special thanks are given to Shenmu Erosion and Environment Research Station for experimental support to this research. We thank Prof. David Dunkerley and two anonymous reviewers for their professional comments, which greatly improve the quality of this manuscript.

Appendix

List of symbols

Abbreviation	Descriptions	Unit
a.s.l.	above sea level	NA
BA	Branch angle	°
BBA	Branch basal area	mm^2
BD	Branch diameter	mm
BL	Branch length	cm
D	Diameter of rain drop	mm
e_s	Saturation vapor pressure	kPa
E	Evaporation coefficient	unitless

F	Average raindrop momentum in the vertical direction of incident event	mg·m·s^{-1}
F_0	Average raindrop momentum of incident event	mg·m·s^{-1}
F_{10}	The 10-min maximum raindrop momentum	mg·m·s^{-1}
F_{b10}	Average raindrop momentum at the first 10 min	mg·m·s^{-1}
F_{e10}	Average raindrop momentum at the last 10 min	mg·m·s^{-1}
FR	Average funnelling ratio of incident event	unitless
FR_{100}	Funnelling ratio at the 100-s intervals after rain begins	unitless
H	Air relative humidity	%
I	Average rainfall intensity of incident event	mm·h^{-1}
I_{10}	The 10-min maximum rainfall intensity	mm·h^{-1}
I_{b10}	Average rainfall intensity at the first 10-min of incident event	mm·h^{-1}
I_{e10}	Average rainfall intensity at the last 10-min of incident event	mm·h^{-1}
IW_A	The adjusted inflow water at TBRG	mm
IW_R	The recorded inflow water at TBRG	mm
LA	Leaf area of individual branch	cm^2
MAP	Mean annual precipitation	mm
MCA	Multiple correspondence analysis	NA
NA	Not applicable	NA
p	Level of significance	NA
R^2	Coefficient of determination	NA
RA	Rainfall amount	mm
RD	Rainfall duration	h
RI	Rainfall interval	h
SE	Standard error	NA
SFD	Stemflow duration from its beginning to ending	h
SFI	Average stemflow intensity of incident event	mm·h^{-1}
SFI_{10}	The 10-min maximum stemflow intensity of incident event	mm·h^{-1}
SFI_i	Instantaneous stemflow intensity	mm·h^{-1}
SF_{RG}	Stemflow depth recorded by TBRG	mm
SFV	Stemflow volume	mL
t_i	Time intervals between neighboring tips	h
T	Air temperature	°C
TBRG	Tipping bucket rain gauge	NA
TLE	Time lag of stemflow ending to rainfall ceasing	min
TLG	Time lag of stemflow generation to rainfall beginning	min
TLM	Time lag of stemflow maximization to rainfall beginning	min
v	Terminal velocity of rain drop	m·s^{-1}
VPD	Vapor pressure deficit	kPa
WS	Wind speed	m·s^{-1}
ρ	Density of freshwater at standard atmospheric pressure and 20°C	g·cm^{-3}
θ	Inclination angle of rain drop	°

References

André, F., Jonard, M. and Ponette, Q.: Influence of species and rain event characteristics on stemflow volume in a temperate mixed oak-beech stand, Hydrol. Process., 22, 4455–4466. https://doi.org/10.1002/hyp.7048, 2008.

Bassette, C. and Bussière, F.: Partitioning of splash and storage during raindrop impacts on banana leaves, Agr., Forest Meteorol., 148, 991–1004, https://doi.org/10.1016/j.agrformet.2008.01.016, 2008.

Bittar, T.B., Pound, P., Whitetree, A., Moore, L.D. and van Stan John, T.: Estimation of throughfall and stemflow bacterial flux in a subtropical oak-cedar forest. Geophys. Res. Lett., 45, 1410–1418, https://doi.org/10.1002/2017GL075827, 2018.

Brandt, C.J.: Simulation of the size distribution and erosivity of raindrops and throughfall drops. Earth. Surf. Proc. Land., 15, 687–698, https://doi.org/10.1002/esp.3290150803, 1990.

Bundt, M., Widmer, F., Pesaro, M., Zeyer, J. and Blaser, P.: Preferential flow paths: biological 'hot spots' in soils. Soil. Biol. Biochem., 33, 729–738, https://doi.org/10.1016/S0038-0717(00)00218-2, 2001.

Carlyle-Moses, D.E., Iida, S.I., Germer, S., Llorens, P., Michalzik, B., Nanko, K., Tischer, A. and Levia, D.F.: Expressing stemflow commensurate with its ecohydrological importance, Adv. Water Resources, 121, 472–479, https://doi.org/10.1016/j.advwatres.2018.08.015, 2018.

Carlyle-Moses, D.E. and Price, A.G.: Growing-season stemflow production within a deciduous forest of southern Ontario, Hydrol. Process., 20, 3651–3663, https://doi.org/10.1002/hyp.6380, 2006.

Carlyle-Moses, D.E. and Schooling, J.: Tree traits and meteorological factors influencing the initiation and rate of stemflow from isolated deciduous trees, Hydrol. Process., 29, 4083–4099, https://doi.org/10.1002/hyp.10519, 2015.

Carlyle-Moses, D.E., Park, A.D. and Cameron, J.L.: Modelling rainfall interception loss in forest restoration trials in Panama, Ecohydrology, 3, 272–283, https://doi.org/10.1002/eco.105, 2010.

Cayuela, C., Llorens, P., Sánchez-Costa, E., Levia, D.F. and Latron, J.: Effect of biotic and abiotic factors on inter- and intra-event variability in stemflow rates in oak and pine stands in a Mediterranean mountain area, J. Hydrol., 560, 396–406, https://doi.org/10.1016/j.jhydrol.2018.03.050, 2018.

Corti, G., Agnelli, A., Cocco, S., Cardelli, V., Masse, J. and Courchesne, F.: Soil affects throughfall and stemflow under Turkey oak (*Quercus cerris* L.), Geoderma, 333, 43–56, https://doi.org/10.1016/j.geoderma.2018.07.010, 2019.

Dawoe, E.K., Barnes, V.R. and Oppong, S.K.: Spatio-temporal dynamics of gross rainfall partitioning and nutrient fluxes in shaded-cocoa (*Theobroma cocoa*) systems in a tropical semi-deciduous forest, Agroforst. Syst., 92, 397–413, https://doi.org/10.1007/s10457-017-0108-3, 2018.

Dunkerley, D.L.: Stemflow production and intrastorm rainfall intensity variation: an experimental analysis using laboratory rainfall simulation, Earth. Surf. Proc. Land., 39, 1741–1752, https://doi.org/10.1002/esp.3555, 2014.

Dunkerley, D.L.: Stemflow on the woody parts of plants: dependence on rainfall intensity and event profile from laboratory simulations, Hydrol. Process., 28, 5469–5482, https://doi.org/10.1002/hyp.10050, 2014.

Dunkerley, D.L.: Rainfall intensity bursts and the erosion of soils: an analysis highlighting the need for high temporal resolution rainfall data for research under current and future climates, Earth Surf. Dynam., 7, 345–360, https://doi.org/10.5194/esurf-7-345-2019, 2019.

Durocher, M.G.: Monitoring spatial variability of forest interception, Hydrol. Process., 4, 215–229, https://doi.org/10.1002/hyp.3360040303, 1990.

Fan, J.L., Baumgartl, T., Scheuermann, A. and Lockington, D.A.: Modeling effects of canopy and roots on soil moisture and deep drainage. Vadose. Zone. J., 14, 1–18, https://doi.org/10.2136/vzj2014.09.0131, 2015.

Firn, R.: Plant intelligence: an alternative point of view, Ann. Bot., 93, 345–351, https://doi.org/10.1093/aob/mch058, 2004.

Gao, X.D., Zhao, X.N., Pan, D.L., Yu, L.Y. and Wu, P.T.: Intra-storm time stability analysis of surface soil water content, Geoderma, 352, 33–37, https://doi.org/10.1016/j.geoderma.2019.06.001, 2019.

Garbelotto, M.M., Davidson, J.M., Ivors, K., Maloney, P.E., Hüberli, D., Koike, S.T. and Rizzo, D.M.: Non-oak native plants are main hosts for sudden oak death pathogen in California, Calif. Agric, 57, 18–23, https://doi.org/10.3733/ca.v057n01p18, 2003.

Germer, S.: Development of near-surface perched water tables during natural and artificial stemflow generation by babassu palms, J. Hydrol., 507, 262–272, http://dx.doi.org/10.1016/j.jhydrol.2013.10.026, 2013.

Germer, S., Werther, L. and Elsenbeer, H.: Have we underestimated stemflow? Lessons from an open tropical rainforest, J. Hydrol., 395, 169–179, https://doi.org/10.1016/j.jhydrol.2010.10.022, 2010.

Giacomin, A. and Trucchi, P.: Rainfall interception in a beech coppice (Acquerino, Italy). J. Hydrol., 137, 141–147, https://doi.org/10.1016/0022-1694(92)90052-W, 1992.

Groisman, P.Y. and Legates, D.R.: The accuracy of United States precipitation data, B. Am. Meteorol. Soc., 75, 215–227, https://doi.org/10.1175/1520-0477(1994)075<0215:TAOUSP>2.0.CO;2, 1994.

Hair, J.F., Anderson, R.E., Tatham, R.L. and Black, W.C.: Multivariate Data Analysis, fourth ed. Prentice Hall College Division, 745 p, 1995.

Herwitz, S.R.: Infiltration-excess caused by Stemflow in a cyclone-prone tropical rainforest, Earth Surf. Proc. Land, 11, 401–412, https://doi.org/10.1002/esp.3290110406, 1986.

Hill, T. and Lewicki, P.: Statistics: Methods and Applications. Statsoft, Tulsa, 800 p, 2007.

Hu, R., Wang, X.P., Zhang, Y.F., Shi, W., Jin, Y.X. and Chen, N.: Insight into the influence of sand-stabilizing shrubs on soil enzyme activity in a temperate desert, Catena, 137, 526–535, http://dx.doi.org/10.1016/j.catena.2015.10.022, 2016.

Iida, S., Levia, D.F., Shimizu, A., Shimizu, T., Tamai, K., Nobuhiro, T., Kabeya, N., Noguchi, S., Sawano, S. and Araki, M.: Intrastorm scale rainfall interception dynamics in a mature coniferous forest stand, J. Hydrol., 548, 770–783, https://doi.org/10.1016/j.jhydrol.2017.03.009, 2017.

Iida, S., Shimizu, T., Kabeya, N., Nobuhiro, T., Tamai, K., Shimizu, A., Ito, E., Ohnuki, Y., Abe, T., Tsuboyama, Y., Chann, S. and Keth, N.: Calibration of tipping-bucket flow meters and rain gauges to measure gross rainfall, throughfall, and stemflow applied to data from a Japanese temperate coniferous forest and a Cambodian tropical deciduous forest, Hydrol. Process., 26, 2445–2454, https://doi.org/10.1002/hyp.9462, 2012.

Jia, X.X., Shao, M.A., Wei, X.R. and Wang, Y. Q.: Hillslope scale temporal stability of soil water storage in diverse soil layers, J. Hydrol., 498, 254–264, https://doi.org/10.1016/j.jhydrol.2013.05.042, 2013.

Johnson, M.S. and Lehmann, J.: Double-funneling of trees: Stemflow and root-induced preferential flow, Ecoscience, 13, 324–333, https://doi.org/0.2980/i1195-6860-13-3-324.1, 2006.

Kéfi, S., Rietkerk, M., Alados, C.L., Pueyo, Y., Papanastasis, V.P., ElAich, A. and De Ruiter, P.C.: Spatial vegetation patterns and imminent desertification in Mediterranean arid ecosystems, Nature, 449, 213–217, https://doi.org/10.1038/nature06111, 2007.

Kimble, P.D.: Measuring the momentum of throughfall drops and raindrops. Master Thesis. Western Kentucky University, Bowling Green, 126 pp, 1996.

Levia, D.F. and Germer, S.: A review of stemflow generation dynamics and stemflow-environment interactions in forests and shrublands, Rev. Geophys., 53, 673-714, 2015, https://doi.org/10.1002/2015RG000479, 2015.

Levia, D.F., van Stan, J.T., Mage, S.M. and Kelley-Hauske, P.W.: Temporal variability of stemflow volume in a beech-yellow poplar forest in relation to tree species and size, J. Hydrol., 380, 112–120, https://doi.org/10.1016/j.jhydrol.2009.10.028, 2010.

Liang, W.L., Kosugi, K. and Mizuyama, T.: Soil water dynamics around a tree on a hillslope with or without rainwater supplied by stemflow, Water Resour. Res., https://doi.org/10.1029/2010WR009856, 2011.

Liang, W.L., Kosugi, K. and Mizuyama, T.: Soil water redistribution processes around a tree on a hillslope: the effect of stemflow on the drying process, Ecohydrology, 8, 1381–1395, https://doi.org/10.1002/eco.1589, 2014.

Li X., Xiao, Q.F., Niu, J.Z., Dymond, S., van Doorn, N.S., Yu, X.X., Xie, B.Y., Lv, X.Z., Zhang, K.B. and Li, J.: Process-based rainfall interception by small trees in Northern China: The effect of rainfall traits and crown structure characteristics, Agric. For. Meteorol., 218–219, 65–73, https://doi.org/10.1016/j.agrformet.2015.11.017, 2016.

Li, X.Y., Liu, L.Y., Gao, S.Y., Ma, Y.J. and Yang, Z.P.: Stemflow in three shrubs and its effect on soil water enhancement in semiarid loess region of China, Agric. For. Meteorol., 148, 1501–1507, https://doi.org/10.1016/j.agrformet.2008.05.003, 2008.

Li, Y.Y., Chen, W.Y., Chen, J.C. and Shi, H.: Contrasting hydraulic strategies in *Salix psammophila* and *Caragana korshinskii* in the southern Mu Us Desert, China, Ecol. Res., 31, 869–880, https://doi.org/10.1007/s11284-016-1396-1, 2016.

Liu, Y.X., Zhao, W.W., Wang, L.X., Zhang, X., Daryanto, S. and Fang, X.N.: Spatial variations of soil moisture under *Caragana korshinskii* kom. from different precipitation zones: field based analysis in the Loess Plateau, China, Forests, 7, https://doi.org/10.3390/f7020031, 2016.

Magliano, P.N., Whitworth-Hulse, J.I. and Baldi, G.: Interception, throughfall and stemflow partition in drylands: Global synthesis and meta-analysis, J. Hydrol., 568, 638–645, https://doi.org/10.1016/j.jhydrol.2018.10.042, 2019.

Manfroi, O.J., Koichiro, K., Nobuaki, T., Masakazu, S., Nakagawa, M., Nakashizuka, T. and Chong, L.: The stemflow of trees in a Bornean lowland tropical forest, Hydrol.

Process., 18, 2455–2474, https://doi.org/10.1002/hyp.1474, 2004.

Martinez-Meza, E. and Whitford, W.: Stemflow, throughfall and channelization of stemflow by roots in three Chihuahuan desert shrubs, J. Arid Environ., 32, 271–287, https://doi.org/10.1006/jare.1996.0023, 1996.

Mcclain, M.E., Boyer, E.W., Dent, C.L., Gergel, S.E., Grimm, N.B., Groffman, P.M., Hart, S.C., Harvey, J.W., Johnston, C.A. and Mayorga, E.: Biogeochemical hot spots and hot moments at the interface of terrestrial and aquatic ecosystems, Ecosystems, 6, 301–312, https://doi.org/10.1007/s10021-003-0161-9, 2003.

Návar, J.: Stemflow variation in Mexico's northeastern forest communities: Its contribution to soil moisture content and aquifer recharge, J. Hydrol., 408, 35–42, https://doi.org/10.1016/j.jhydrol.2011.07.006, 2011.

Owens, M.K., Lyons, R.K. and Alejandro, C.L.: Rainfall partitioning within semiarid juniper communities: effects of event size and canopy cover, Hydrol. Process., 20, 3179–3189, https://doi.org/10.1002/hyp.6326, 2006.

Reid, L.M. and Lewis, J.: Rates, timing, and mechanisms of rainfall interception loss in a coastal redwood forest, J. Hydrol., 375, 459–470, https://doi.org/10.1016/j.jhydrol.2009.06.048, 2009.

Schimmack, W., Förster, H., Bunzl, K., and Kreutzer, K.: Deposition of radiocesium to the soil by stemflow, throughfall and leaf-fall from beech trees, Radiat. Environ. Bioph., 32, 137–150, https://doi.org/10.1007/bf01212800, 1993.

Siegert, C.M. and Levia, D.F.: Seasonal and meteorological effects on differential stemflow funneling ratios for two deciduous tree species, J. Hydrol., 519, 446–454, https://doi.org/10.1016/j.jhydrol.2014.07.038, 2014.

Spencer, S.A. and van Meerveld, H.J.: Double funnelling in a mature coastal British Columbia forest: spatial patterns of stemflow after infiltration, Hydrol. Process., 30, 4185–4201, https://doi.org/10.1002/hyp.10936, 2016.

Sprenger, M., Stumpp, C., Weiler, M., Aeschbach, W., Allen, S.T., Benettin, P., Dubbert, M., Hartmann, A., Hrachowitz, M., Kirchner, J.W., McDonnell, J.J., Orlowski, N., Penna, D., Pfahl, S., Rinderer, M., Rodriguez, N., Schmidt, M. and Werner, C.: The Demographics of Water: A Review of Water Ages in the Critical Zone, Rev. Geophys., 57, 1–35, https://doi.org/10.1029/2018RG000633, 2019.

Staelens, J., De Schrijver, A., Verheyen, K. and Verhoest N.E.: Rainfall partitioning into throughfall, stemflow, and interception within a single beech (*Fagus sylvatica* L.) canopy: influence of foliation, rain event characteristics, and meteorology, Hydrol. Process., 22, 33–45, https://doi.org/10.1002/hyp.6610, 2008.

Teachey, M.E., Pound, P., Ottesen, E.A. and van Stan, J.T.: Bacterial community composition of throughfall and stemflow, Front. Plant. Sci., 1, 1–6, https://doi.org/10.3389/ffgc.2018.00007, 2018.

Uijlenhoet, R. and Sempere Torres, D.: Measurement and parameterization of rainfall microstructure, J. Hydrol., 328, 1, 1–7, https://doi.org/10.1016/j.jhydrol.2005.11.038, 2006.

van Stan, J.T. and Levia, D.F.: Inter- and intraspecific variation of stemflow production from *Fagus grandifolia* Ehrh. (American beech) and *Liriodendron tulipifera* L. (yellow poplar) in relation to bark microrelief in the eastern United States, Ecohydrology, 3, 11–19, https://doi.org/10.1002/eco.83, 2010.

van Stan, J.T., Siegert, C.M., Levia D.F. and Scheick, C.E.: Effects of wind-driven rainfall on stemflow generation between codominant tree species with differing crown characteristics, Agric. For. Meteorol., 151, 9, 1277–1286, https://doi.org/10.1016/j.agrformet.2011.05.008, 2011.

van Stan, J.T., Gay, T.E. and Lewis, E.S.: Use of multiple correspondence analysis (MCA) to identify interactive meteorological conditions affecting relative throughfall, J. Hydrol., 533, 452–460, https://doi.org/10.1016/j.jhydrol.2015.12.039, 2016.

Wang, X.P., Wang, Z.N., Berndtsson, R., Zhang, Y.F. and Pan, Y.X.: Desert shrub stemflow and its significance in soil moisture replenishment, Hydrol. Earth Syst. Sci., 15, 561–567, https://doi.org/10.5194/hess-15-561-2011, 2011.

Yang, Z.P.: Rainfall partitioning process and its effects on soil hydrological processes for sand-fixed shrubs in Mu us sandland, Northwest China. PhD Thesis. Beijing Normal University, Beijing, 123 pp (in Chinese with English abstract), 2010.

Yang, X.L., Shao, M.A. and Wei, X.H.: Stemflow production differ significantly among tree and shrub species on the Chinese Loess Plateau, J. Hydrol., 568, 427–436, https://doi.org/10.1016/j.jhydrol.2018.11.008, 2019.

Yuan, C., Gao, G.Y. and Fu, B.J.: Stemflow of a xerophytic shrub (*Salix psammophila*) in northern China: Implication for beneficial branch architecture to produce stemflow, J. Hydrol., 539, 577–588, https://doi.org/10.1016/j.jhydrol.2016.05.055, 2016.

Yuan, C., Gao, G.Y. and Fu, B.J.: Comparisons of stemflow and its bio-/abiotic influential factors between two xerophytic shrub species, Hydrol. Earth Syst. Sci., 21, 1421–1438, https://doi.org/10.5194/hess-21-1421-2017, 2017.

Zabret, K., Rakovec, J. and Šraj, M.: Influence of meteorological variables on rainfall partitioning for deciduous and coniferous tree species in urban area, J. Hydrol., 558, 29–41, https://doi.org/10.1016/j.jhydrol.2018.01.025, 2018.

Zhang, Y., Li, X.Y., Li, W., Wu, X.C., Shi, F.Z., Fang, W.W. and Pei, T.T.: Modeling rainfall interception loss by two xerophytic shrubs in the Loess Plateau, Hydrol. Process., 31, 1926–1937, https://doi.org/10.1002/hyp.11157, 2017.

Zhang, Y.F., Wang X.P., Hu, R., Pan Y.X. and Paradeloc, M.: Rainfall partitioning into throughfall, stemflow and interception loss by two xerophytic shrubs within a rain-fed re-vegetated desert ecosystem, northwestern China, J. Hydrol., 527, 1084–1095, https://doi.org/10.1016/j.jhydrol.2015.05.060, 2015.

Table 1. Branch morphologies of *C. korshinskii* and *S. psammophila* for stemflow recording.

Shrub species	BD categories (mm)	Branch amount	BD (mm)	BL (cm)	BA (°)	LA (cm^2)
	5–10	2	6.6	131	61	837.1
	10–15	2	13.1	168	43	2577.3
C. korshinskii	15–18	2	17.8	206	72	4243.1
	18–25	1	22.1	242	50	6394.7
	>25	NA	NA	NA	NA	NA
	5–10	2	7.5	248	69	626.3
	10–15	2	13.2	343	80	1683.5
S. psammophila	15–18	NA	NA	NA	NA	NA
	18–25	2	21.8	286	76	3468.3
	>25	1	31.3	356	60	7513.7

Notes: BD, BL and BA are branch basal diameter, length and inclination angle, respectively; LA is leaf area of individual branches; NA means not applicable.

Table 2. Rainfall characteristics during events with different intensity peak amounts.

Indicators	Event A	Event B	Event C	Others	Average
Event amount	17	11	15	11	13.5±1.5
RA (mm)	4.1 ab	5.2 b	11.7 c	0.6 a	5.4 ± 0.9
RD (h)	2.5 a	3.6 a	10.3 b	2.2 a	4.7 ± 0.8
RI (h)	48.5 ab	70.5 b	57.3 ab	26.1 a	50.6 ± 6.1
I ($mm \cdot h^{-1}$)	5.6 a	5.5 a	4.6 a	2.2 b	4.5 ± 1.0
I_{10} ($mm \cdot h^{-1}$)	15.5 a	12.7 ab	9.5 b	6.0 c	10.9 ± 2.1
I_{b10} ($mm \cdot h^{-1}$)	7.7 a	9.9 a	2.8 b	1.6 b	5.5 ± 1.4
I_{e10} ($mm \cdot h^{-1}$)	4.3 a	3.6 a	2.1 ab	1.2 b	2.8 ± 0.7
F ($mg \cdot m \cdot s^{-1}$)	17.1 a	17.6 a	17.2 a	12.5 b	16.1 ± 1.2
F_{10} ($mg \cdot m \cdot s^{-1}$)	27.8 a	26.6 a	24.2 ab	21.0 b	24.9 ± 1.4
F_{b10} ($mg \cdot m \cdot s^{-1}$)	19.7 ab	21.7 a	15.4 b	16.9 b	18.4 ± 1.4
F_{e10} ($mg \cdot m \cdot s^{-1}$)	17.3 a	16.6 a	13.4 b	16.8 a	16.0 ± 1.0
E (unitless)	0.9 ab	1.0 ab	0.4 a	1.7 b	0.9 ± 0.2

Note: Event A, Event B and Event C are events with the single, double and multiple rainfall intensity peaks, respectively; Others are the events that excluded from the categorization; RA, RD and RI are rainfall amount, duration and interval, respectively; I and I_{10} are the average and 10-min maximum rainfall intensities, respectively; I_{b10} and I_{e10} are the average rainfall intensities in 10 min after rain begins and before rain ends, respectively; F and F_{10} are the average and 10-min maximum raindrop momentums, respectively; F_{b10} and F_{e10} are the average raindrop momentums in 10 min after rain begins and before rain ends, respectively; E is evaporation coefficient; Different letters indicate significant differences of rainfall characteristics between event categories ($p<0.05$) (rows at the table).

Table 3. Stemflow variables of *C. korshinskii* and *S. psammophila* during rainfall events with different intensity peak amounts.

Species	Stemflow variables	Event A	Event B	Event C	Others	Average
*C. korshinsk*i	SFV (mL)	134.1 a	203.7 a	560.8 b	7.6 c	226.6 ± 46.4
	SFI (mm·h^{-1})	672.9 a	552.4 b	527.0 b	317.8 c	517.5 ± 82.1
	SFI_{10} (mm·h^{-1})	2849.0 a	2399.3 a	1809.1 b	1173.2 c	2057.6 ± 399.7
	FR (unitless)	109.4 a	146.6 b	137.9 b	128.9 ab	130.7 ± 8.2
	TLG (min)	67.3 ab	56.2 a	67.0 ab	74.2 b	66.2 ± 10.6
	TLM (min)	81.1 a	75.5 a	202.1 b	78.8 a	109.4 ± 20.5
	TLE (min)	22.3 a	18.7 b	18.5 b	20.6 a	20.0 ± 5.3
	SFD (h)	1.4 a	3.1 a	9.1 b	1.4 a	3.8 ± 0.8
S. psammophila	SFV (mL)	102.6 a	145.7 a	435.2 b	4.7 c	172.1 ± 34.5
	SFI (mm·h^{-1})	648.1 a	421.5 b	246.6 c	153.2 c	367.3 ± 91.1
	SFI_{10} (mm·h^{-1})	1672.7 a	1582.8 a	888.4 b	384.7 c	1132.2 ± 214.3
	FR (unitless)	77.1 a	91.4 a	129.1 b	101.6 ab	101.6 ± 10.4
	TLG (min)	84.9 a	46.5 b	56.1 b	31.5 b	54.8 ± 11.7
	TLM (min)	64.3 a	93.4 a	235.8 b	88.4 a	120.5 ± 22.1
	TLE (min)	17.1 a	8.6 b	20.8 a	7.3 b	13.5 ± 17.2
	SFD (h)	1.2 a	3.4 a	8.3 b	0.7 a	3.4 ± 0.9

Note: Event A, Event B and Event C are events with the single, double and multiple rainfall intensity peaks, respectively; Others are the events that excluded from the categorization; SFV is stemflow volume; SFI and SFI_{10} are the average and 10-min maximum stemflow intensities at incident rains, respectively; FR is funnelling ratio of stemflow at incident rains; TLG and TLM are time lags of stemflow generating and maximizing after rains begin, respectively; TLE is time lag of stemflow ending after rain ceases; SFD is stemflow duration; Different letters indicate significant differences of stemflow variables between event categories (p<0.05) (rows at the table).

Table 4. Comparisons of stemflow intensity and funnelling ratio at different basal diameter categories.

Species and stemflow variables		BD categories (mm)					
		5–10	10–15	15–18	18–25	>25	AVG
C. korshinskii	FR	163.7±12.2a	136±10.9b	119.5±13.0b	97.7±9.2b	NA	131±8.2
	SFI	716.2±118.7a	552.5±90.3b	619±103.3b	333.8±45.8b	NA	553.9±82.1
S. psammophila	FR	212±17.4a	84±6.4b	NA	44.2±3.0b	54.9±4.2b	100.6±7.9
	SFI	738.7±160.9a	360.7±82.7a	NA	197.2±44.9b	209.9±44.5b	372.2±79.4

Note: SFI and FR are the average stemflow intensity and funnelling ratio at incident rains, respectively; BD is branch basal diameter (mm); NA means not applicable; Different letters indicate significant differences of stemflow variables between event categories ($p<0.05$) (rows at the table).

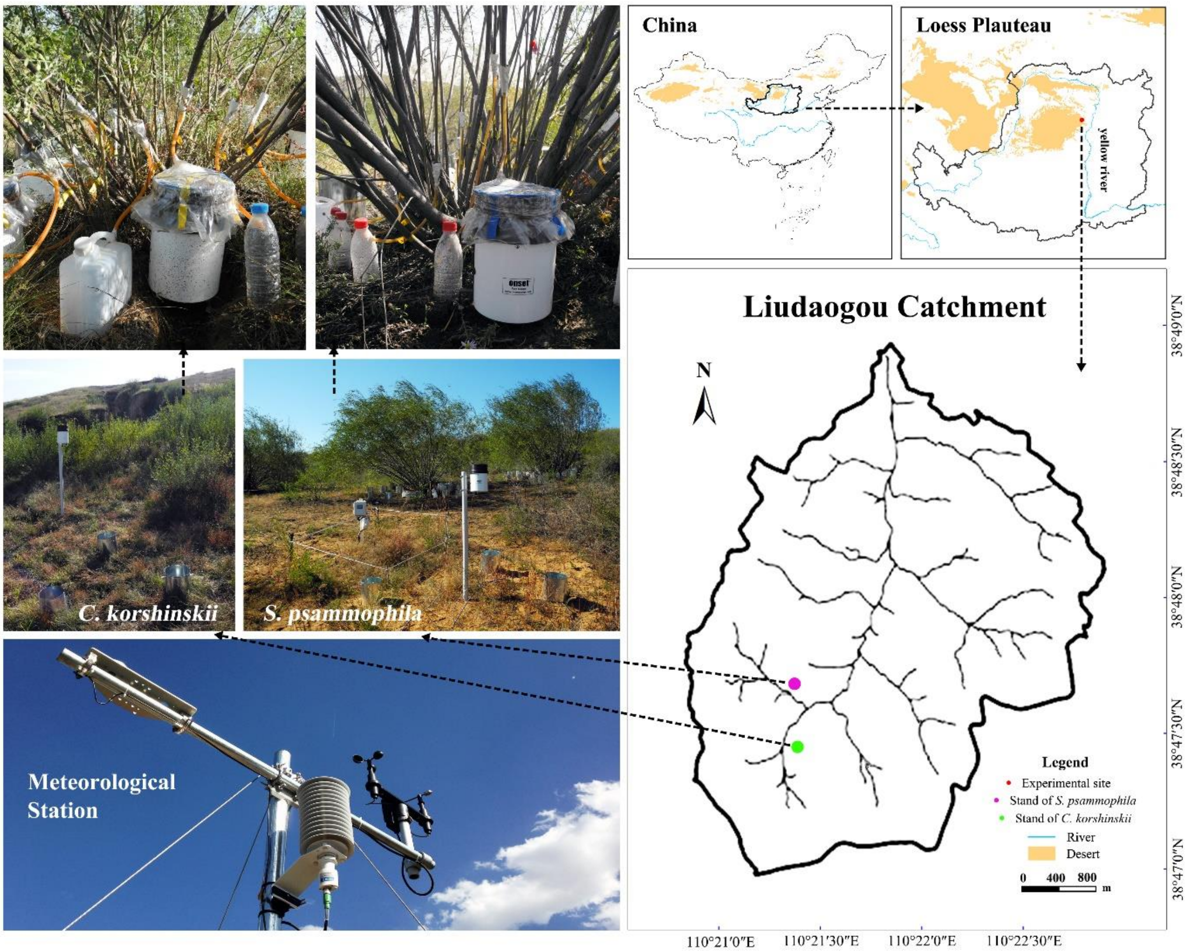

Figure 1. Locations and experimental settings in the plots of *C. korshinskii* and *S. psammophila*.

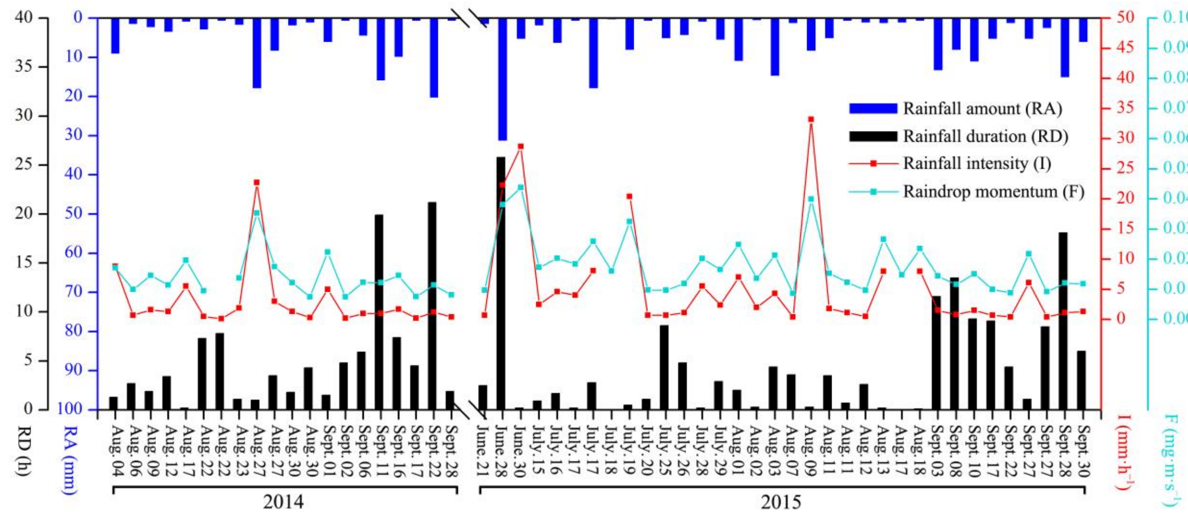

Figure 2. Inter-event variations in rainfall characteristics during the experimental period.

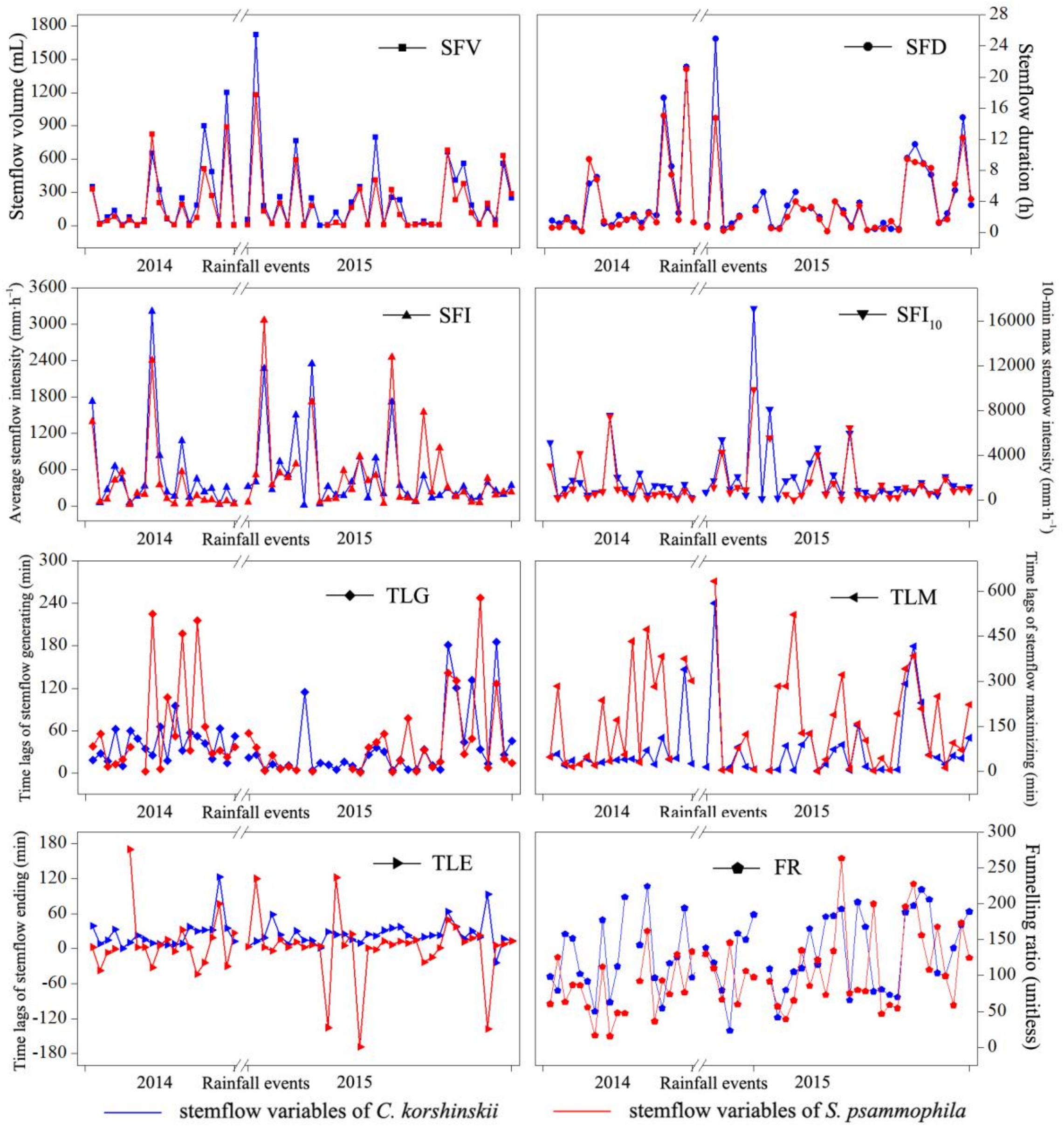

Figure 3. Inter-event variations in stemflow variables of *C. korshinskii* and *S. psammophila* during the experimental period.

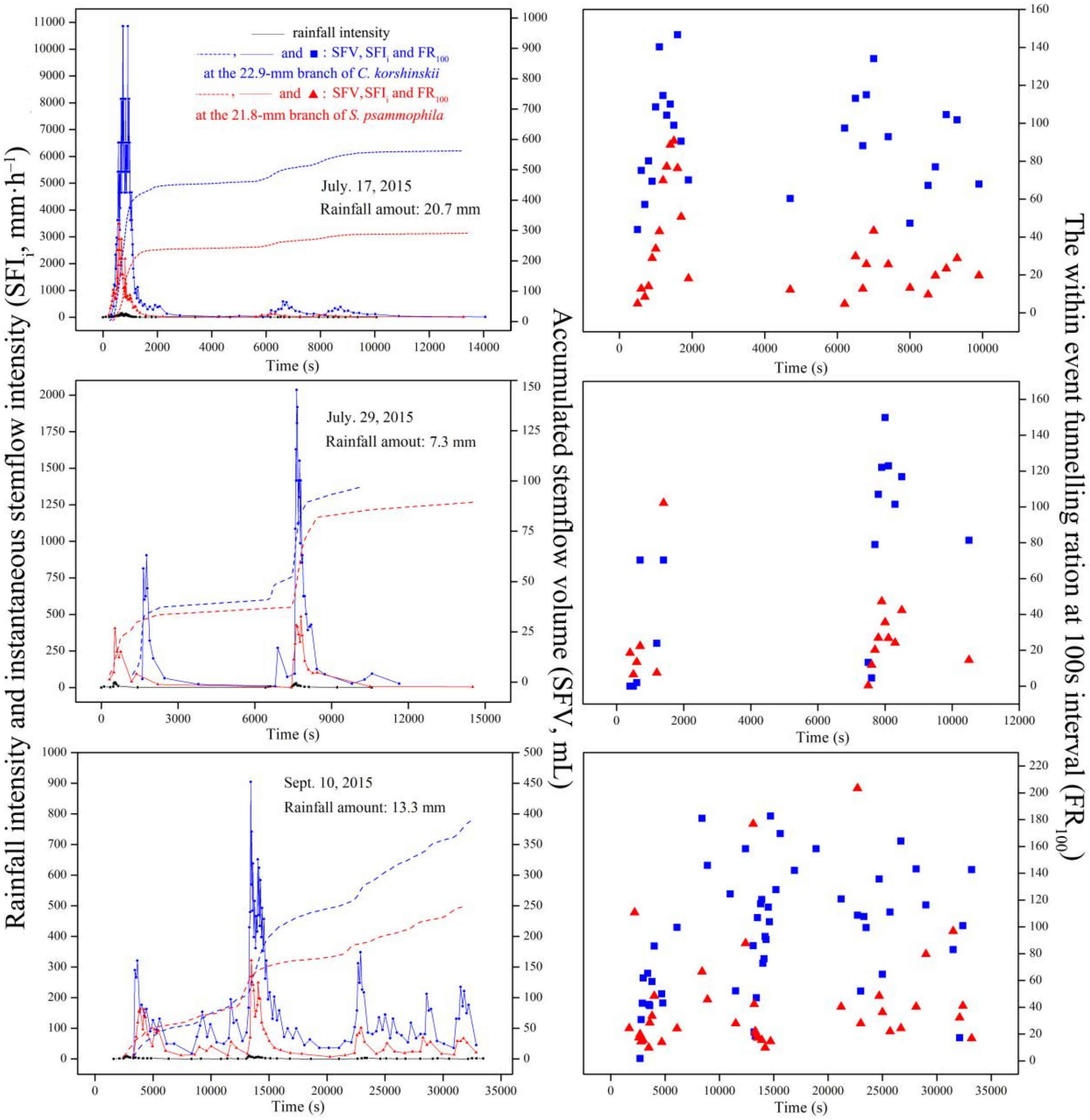

Figure 4. Stemflow synchronicity of *C. korshinskii* and *S. psammophila* to rains during representative events with different rainfall-intensity peak amounts.

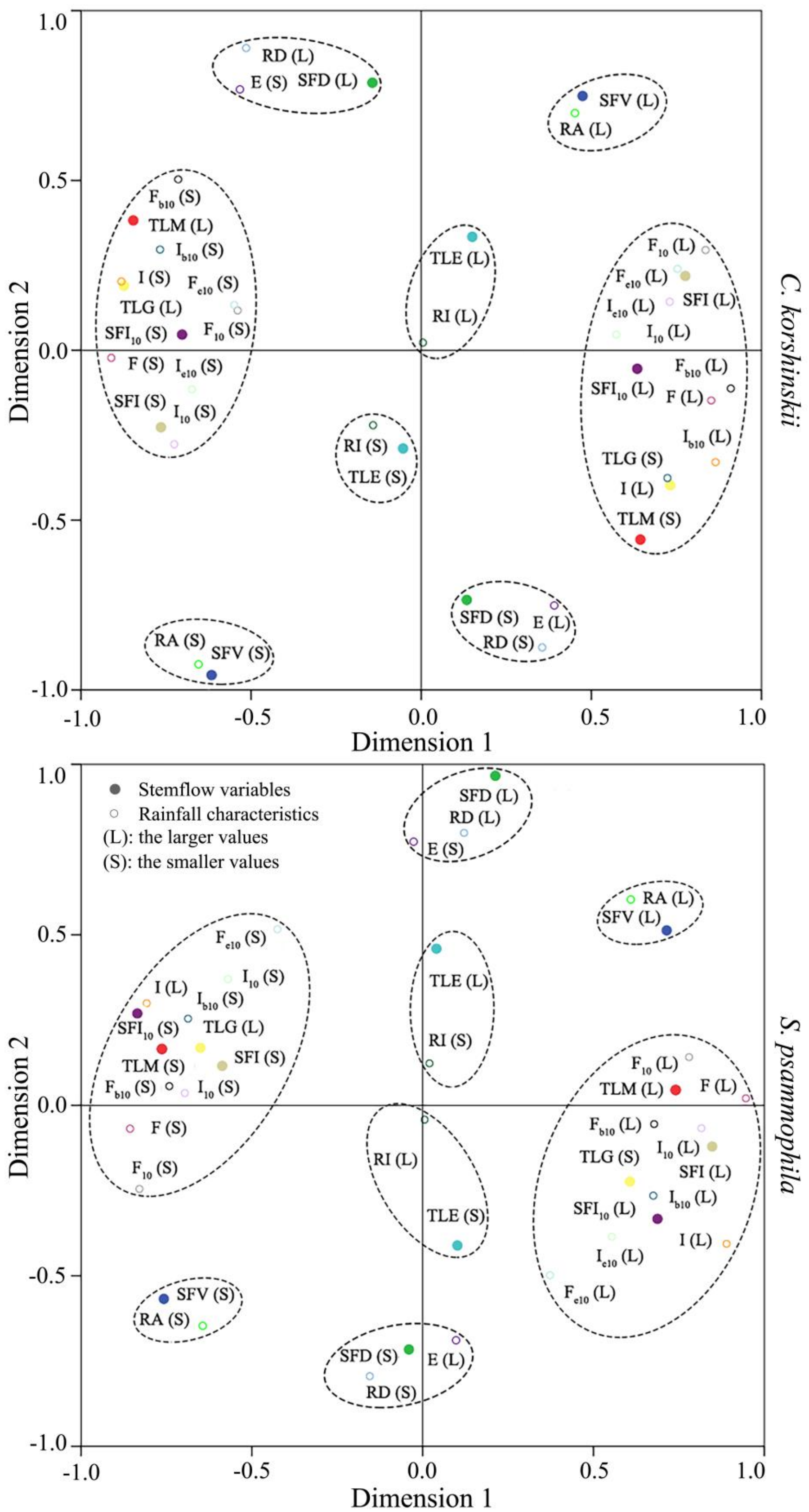

Figure 5. Correspondence maps of stemflow variables with rainfall characteristics for *C. korshinskii* and *S. psammophila*.

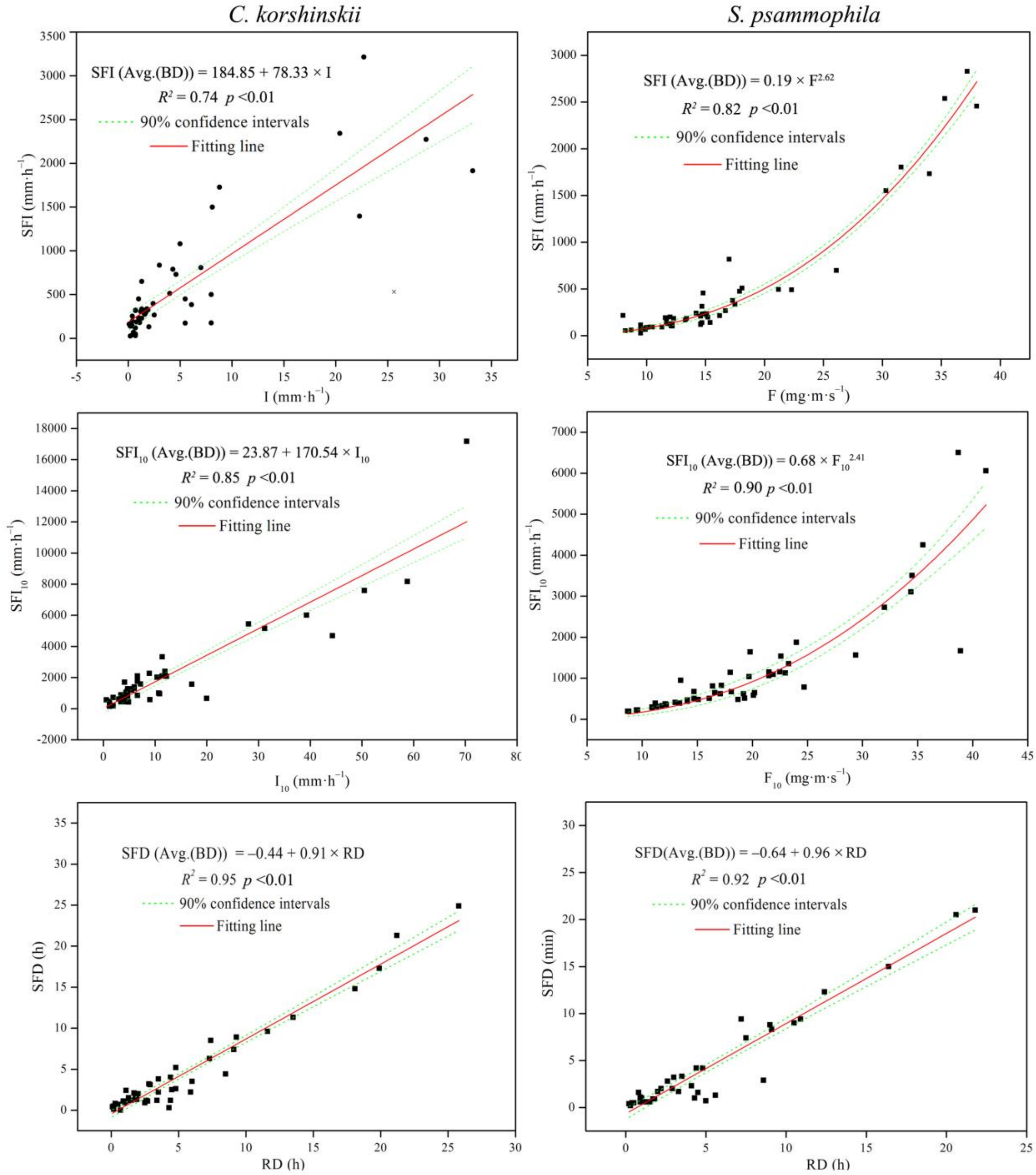

Figure 6. Relationships of stemflow intensity and duration with rainfall characteristics.

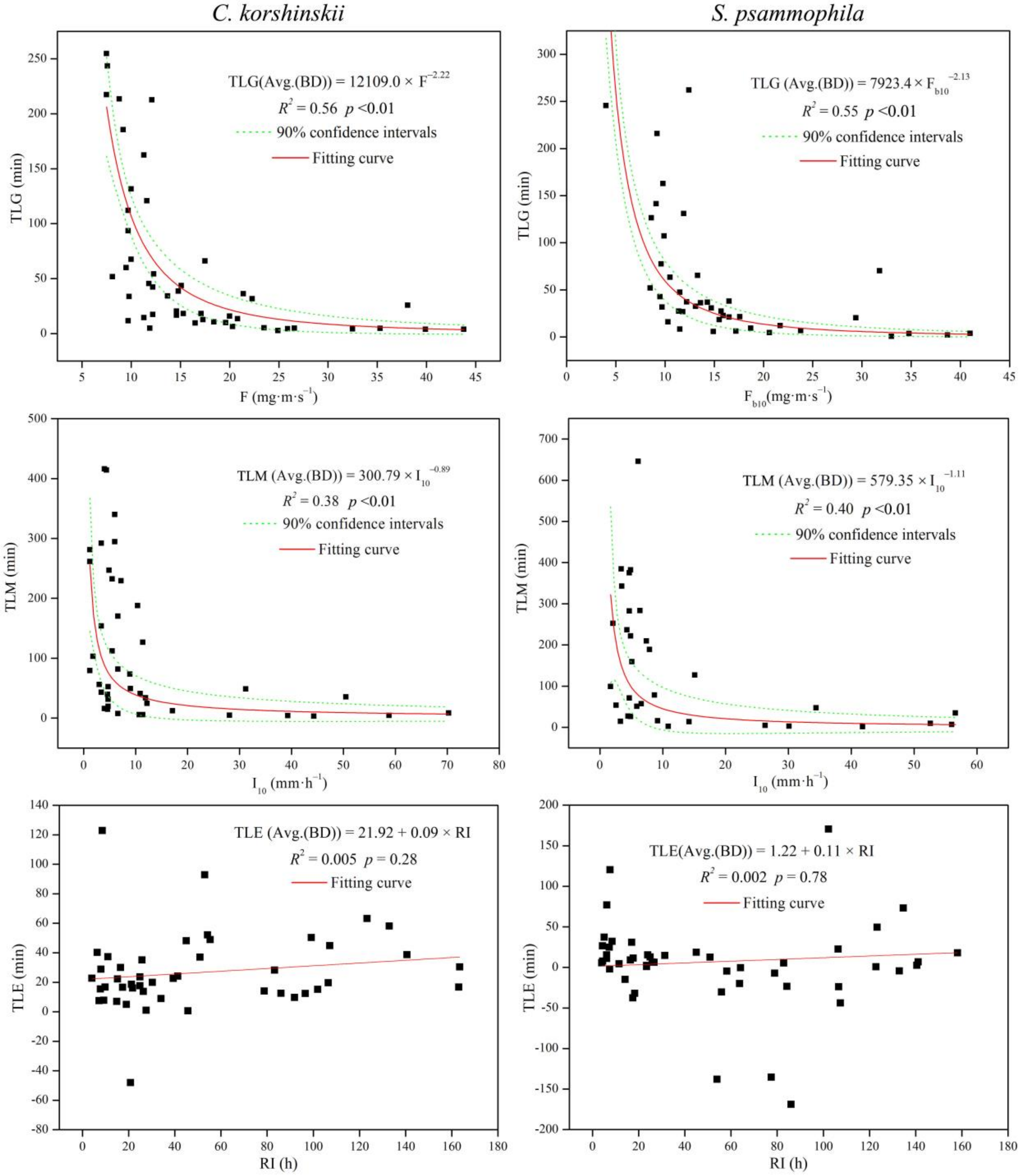

Figure 7. Relationships of stemflow time lags with rainfall characteristics.